Journal of Alloys and Compounds 502 (2010) 1–4

Contents lists available at ScienceDirect

Journal of Alloys and Compounds

journal homepage: www.elsevier.com/locate/jallcom

Fabrication and magnetic properties of Fe–6.5% Si alloys by magnetron sputtering method

Guangke Tian, Xiaofang Bi *

Key Laboratory of Aerospace Materials and Performance (Ministry of Education), School of Materials Science and Engineering, Beijing University of Aeronautics and Astronautics, #37 Xueyuan Road, Beijing 100191, China

ARTICLE INFO

Article history:
Received 2 December 2009
Received in revised form 20 February 2010
Accepted 26 February 2010
Available online 4 March 2010

Keywords:
Fe–6.5% Si alloys
Physical vapor deposition
Diffusion
SEM
TEM

ABSTRACT

Two-side deposition approach was applied to prepare Si-enriched FeSi alloys from 3% Si starting sheets with 0.35 mm thickness. FeSi layer was first deposited by direct current (DC) magnetron sputtering on the alloy, which was then subjected to vacuum annealing. It is found that reduction of the deposited FeSi layer thickness suppresses evaporation of Si during the annealing process, which is of great significance in enhancing efficiency of Si penetration into the low-Si starting alloy. After the Si-enriched process, the alloys demonstrate dense and uniform microstructure with 6.5% Si and exhibit α-Fe(Si) bcc structure revealed by X-ray diffractometer (XRD) and transmission electron microscope (TEM). Iron losses of the PVD-prepared Fe–6.5% Si alloy are as low as those of the alloys fabricated by CVD.

© 2010 Elsevier B.V. All rights reserved.

1. Introduction

The Fe–6.5% (weight percentage) Si alloy has attracted considerable interest due to its high permeability, high saturation magnetization and zero magnetostriction. In addition, electrical resistivity of the Si-enriched alloy is higher and expected to have lower core losses than conventional Fe–3% Si steel sheets. However, the high-Si alloys are known to be quite brittle, which brings about difficulty in conventional hot–cold rolling processes [1–5]. Several techniques such as rapid quenching [6–8], spray forming [9] and chemical vapor deposition (CVD) [10] etc. were developed to overcome the drawbacks, in an attempt to produce Fe–6.5% Si thin sheets required by electromagnetic applications. The rapid quenching approach was applied due to its possibility to produce ribbon products that are characterized by good mechanical properties. However, the techniques including spray forming suffer uneven thickness and size limitations of products, which brings about difficulty in sheet-stacking for fabrication of electrical parts [9]. In contrast to this, high-Si alloys can be obtained through the CVD siliconizing process with controllable size such as thickness and width. Therefore, the Si-enriched technique has been, up to date, widely applied in the production of the alloys on a commercial scale. However, in the wake of growing environmental awareness, it is of significance to develop a technique by which harmful by-products accompanied with the CVD process can be avoided. Physical vapor deposition (PVD) technique by magnetron sputtering is known to have many advantages over CVD such as environmental friendliness, energy-saving, purification controlling, and therefore it has been developed and applied successfully in many industrial fields [11–14]. It is considered that the PVD method could be a promising and feasible approach in fabrication of high-Si alloys. Aldareguia et al. reported that Si was deposited on 0.25 mm thick Fe–3% Si electrical steels using magnetron sputtering and the processed alloys contained less than 4% Si [15]. In this work, we have prepared Fe–6.5% Si sheets based on the processes including magnetron sputtering deposition of FeSi layers onto conventional Fe–3% Si steel sheets and subsequent annealing treatment. Si penetration efficiency was studied to optimize the deposition and diffusion parameters, and magnetic properties of the Fe–6.5% Si alloys were investigated in comparison with commercial counterparts manufactured by CVD technique.

2. Experimental

0.35 mm thick Si steel sheets with 3% Si content were cut for starting substrates into two sizes: 10 mm × 10 mm samples used for the analysis of structures and Si penetration effect; ring samples with outer and inner diameter of 19 mm and 9 mm for the measurement of magnetic properties. The target is an arc-melt FeSi alloy with 23% Si. FeSi layers of 90 μm and 15 μm thicknesses were deposited onto single-side surface of the substrates by DC magnetron sputtering, followed by annealing at 1180 °C for 1 h and 2 h respectively to evaluate Si penetration efficiency. Table 1 lists the detail deposition parameters. Structure was characterized by X-ray diffractometer (XRD) D/max2200PC, Rigaku with Cu Ka radiation and 200 kV field-emission high-resolution transmission electron microscopy (HRTEM, 2100F, JEOL), respectively. Cross-sectional compositions and microstructures were analyzed by S-530

* Corresponding author. Tel.: +86 10 82339231.
E-mail address: bixf@buaa.edu.cn (X. Bi).

0925-8388/$ – see front matter © 2010 Elsevier B.V. All rights reserved.
doi:10.1016/j.jallcom.2010.02.175

Table 1
Detail parameters of deposition processes.

Ar pressure (Pa)	Power density (W/mm^2)	Target–substrate spacing (mm)	Substrate temperature (°C)	Deposition rate (nm/min)
0.8	5.4	30	200	84

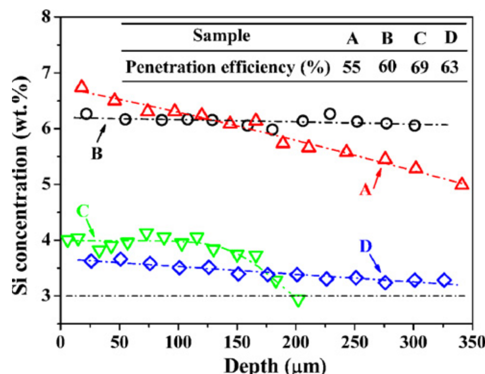

Fig. 1. Cross-sectional Si concentration profiles for the 0.35 mm thick Fe–3% Si alloys deposited with FeSi films ("A" and "B" with 90 μm, "C" and "D" with 15 μm), followed by annealings at 1180 °C for 1 h ("A" and "C") and 2 h ("B" and "D"). The inset lists corresponding Si penetration efficiencies.

scanning electron microscopy (SEM), equipped with Oxford INCA electron dispersive spectrometer (EDS). Resistivity of the samples was measured by four-probe method. Magnetic properties were evaluated by vibrating sample magnetometer (VSM), automatic DC B–H curve tracer and alternating current (AC) iron loss analyzer.

3. Results and discussion

Fig. 1 displays cross-sectional Si concentration profiles for the alloys deposited with FeSi layers, followed by annealing at 1180 °C for 1 h and 2 h, respectively. Here, "A" and "B" represent the samples deposited with 90 μm FeSi, while "C" and "D" refers to those deposited with 15 μm FeSi. In contrast to the gradient distribution of Si contents observed in the samples annealed for 1 h (A and C), the samples annealed for 2 h (B and D) display a nearly uniform distribution of Si. Note that the Si distribution is dominated by annealing time, irrespective of the FeSi thicknesses although the deposited FeSi thicknesses change Si contents in the processed alloys. The processed sample B shows an enriched Si content of 6.2%, indicating that the Si content can be expected to reach up to 6.5% for the samples deposited with FeSi thicknesses >90 μm. Furthermore, we study Si-enriching efficiency (η) for applications into line production, which is defined as following:

$$\eta = \frac{M_{pene}}{M_{depo}} \times 100\%$$

where M_{depo} and M_{pene} represent deposited and penetrated Si amounts, respectively. The Si penetration efficiencies for the samples are listed in the inset of Fig. 1. A distinct result is found that the η increases by reducing the deposited FeSi layer thicknesses onto the substrates. To understand the unexpected findings, we have investigated cross-sectional micrographs and variations of Si contents during annealing for the 15 μm thick FeSi deposited samples. As shown in Fig. 2(a), a good adhesion is seen between the FeSi layer and as-deposited sample. The film reveals a dense microstructure and contains 23% Si, which is consistent with nominal composition of the target. After being annealed at 1050 °C for 1 h, as shown in Fig. 2(b), the sample shows a decrease of the Si content from 23 to 20% in the FeSi layer. However, no obvious Si increment is detected in the substrate. It is known that SiO is volatile at high temperatures [16]. It can be therefore considered that the Si reduction arises from evaporation of the Si at high temperatures in vacuum [17] and/or from partial oxidation of Si on the FeSi layer surface during annealing procedure. The results further indicate that two competitive factors are involved when annealed at higher temperature (such as 1180 °C) and vary Si contents penetrated in the substrate. One is Si diffusion driven by Si concentration gradient between the film and substrate [18], which results in the Si penetration into substrate and increase of Si contents. On the other hand, the unavoidable evaporation and/or micro-oxidation of Si lead to the dissipation of Si. In combination with the Si penetration efficiencies shown in Fig. 1, it can be inferred that thicker FeSi films gives rise to more serious Si evaporations when annealed at high temperatures. Fig. 2(c) shows cross-sectional microstructure for the sample after annealing at 1180 °C for 1 h. The Si distribution is shown by profile C in Fig. 1. It is revealed that the Si penetrated substrate remains a dense and uniform structure. In contrast to this, a porous structure is observed at the substrate-FeSi interface and in the residual film, which is obviously caused by the Kirkendall effect. It should be mentioned that the porous interface is favorable for removing the residual layer from substrate by mechanical polishing. The as-deposited film is characterized by Fe_5Si_3 metastable phase revealed by XRD analysis, as shown in Fig. 3. The result is consistent with Fe–Si binary phase-diagram [19]. The Fe_3Si phase starts to appear after annealing at 1050 °C, while the (1 1 0) peak indexed as α-Fe(Si) is shifted toward right angle sides for the sample annealed at 1180 °C.

Double-side deposition has been furthermore explored to increase the efficiency of Si penetration. The double-side deposition is designated as the process that FeSi is simultaneously deposited on both surfaces of substrate. FeSi layer thickness on each surface is

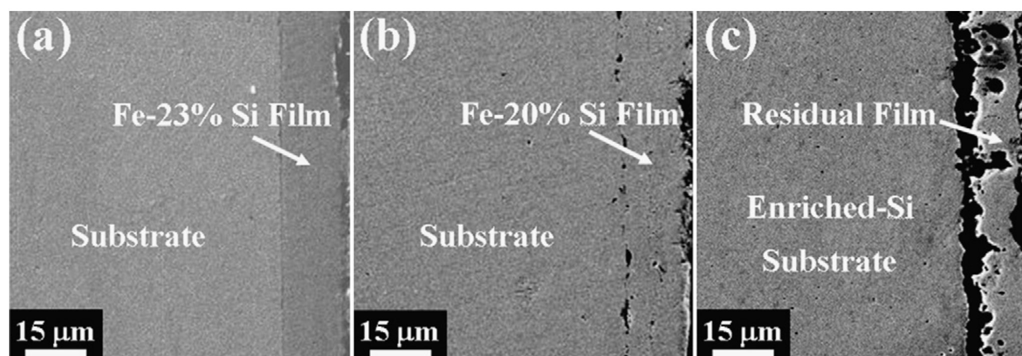

Fig. 2. Cross-sectional SEM images of the samples deposited with 15 μm thick FeSi films: (a) as-deposited, (b) annealed at 1050 °C for 1 h and (c) annealed at 1180 °C for 1 h.

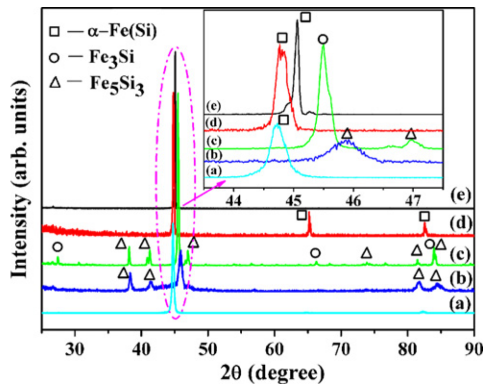

Fig. 3. XRD patterns for (a) starting substrate, (b) as-deposited, (c) annealed at 1050 °C for 1 h, (d) annealed at 1180 °C for 1 h and (e) the fabricated Fe–6.5% Si alloy. The inset magnifies the diffraction profiles in the range of 43.5–47.5°.

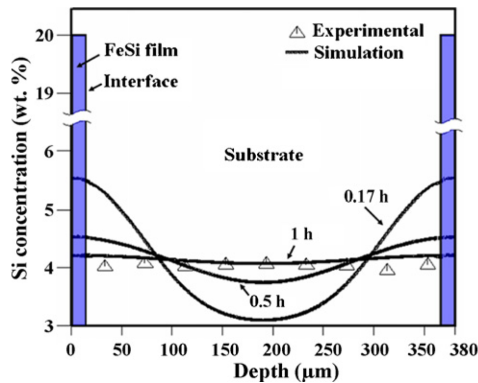

Fig. 4. Si concentration profiles along cross-section of sample deposited onto double-side with 15 μm FeSi and annealed at 1180 °C for 1 h. Solid lines and triangles represent the simulation results and experimental data, respectively. Blue bars show calibrated Si contents of the deposited FeSi layers. (For interpretation of the references to color in this figure legend, the reader is referred to the web version of the article.)

set to be 15 μm. As shown in Fig. 4, the sample annealed at 1180 °C for 1 h contains about 4.1% Si throughout the 0.35 mm thick cross-section. The Si penetration is greatly enhanced by the double-side deposition as compared to the single-side deposition (the profile C as shown in Fig. 1). Penetration efficiency is then evaluated and exhibits a high value of 75%. The enhancement of Si penetration is obviously owing to the double-side deposition, which allows thinner deposited FeSi films and shorter Si diffusion route in the process of Si enrichment as compared to single-side deposition. To obtain variations of Si concentration profiles during diffusion processes, DICTRA simulation can be a useful approach to predict annealing times and temperatures to achieve a desired Si distribution [20]. Cross-sectional Si distributions during annealing at 1180 °C for the double-side deposited samples are simulated by means of DICTRA software, as plotted in Fig. 4. The initial Si content in the FeSi layers was calibrated at 20% by taking into account the Si evaporation. It is seen that Si content is distributed symmetrically along the cross-section throughout the annealing process. The Si-compositional gradient is reduced quickly with annealing time and vanishes with only 1 h annealing, which is in good agreement with experimental data.

To further increase Si contents in the substrate, we have performed multi-round Si penetration process. One round refers to a combination of a double-side deposition of 15 μm thick FeSi with a subsequent annealing at 1180 °C for 1 h. Fig. 5(a) shows cross-sectional Si concentration for the samples processed with different number of rounds. The Si demonstrates uniform distributions independent of the round number, even though the average level of Si content can be increased by increasing the round number. It is seen that 6.5% Si is achieved in the 0.35 mm thick sample processed with four rounds. As revealed by XRD analysis (Fig. 3), the α-Fe(Si) (1 1 0) peak shifts to right angle to a great extent as compared to that of the starting substrate, reflecting the penetration of Si into the substrate. The interplanar distance $d_{(110)}$ is estimated to be 1.995 Å, which is consistent with HRTEM observation, as shown in Fig. 5(b). In addition, super-lattice reflections arising from B2 and DO_3 order phases are detected in the diffraction pattern along the 0 1 1 zone axis [21]. It should be mentioned that no cracks were observed in the mechanically polished specimens. Ductility of the fabricated Fe–6.5% Si alloys needs to be measured to evaluate their mechanical behaviors in the next stage.

Fig. 6(a) shows the DC hysteresis loops of the starting Fe–3% Si sheet and fabricated Fe–6.5% Si alloy. Coercivity estimated from the loops decreases from 35 to 19 A/m for the Fe–6.5% Si as compared to the starting alloy, while maximum permeability exhibits an increase from 11,400 to 16,400. Inset of the figure shows the reduction of Curie temperature with Si contents, which is consistent with previous reports [22]. It is known that, on the other hand, AC magnetic properties of soft magnetic materials are crucial for their industrial applications. As shown in Fig. 6(b), iron loss for the samples, as expected, is reduced monotonously with Si contents. The result can be interpreted by the increase of resistivity with Si contents, as shown in the inset. It is seen that the iron loss of the PVD processed Fe–6.5% Si sheet are reduced by 40–50% as compared to the starting sheet. Furthermore, a comparison regarding iron losses

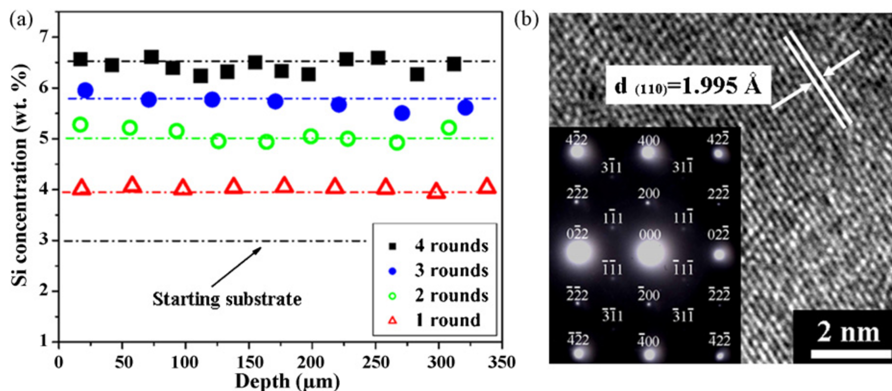

Fig. 5. (a) Si concentration profiles along cross-section of the samples processed by multi-round siliconizing processes and (b) TEM image of the fabricated Fe–6.5% Si alloys and selected area diffraction pattern in the 0 1 1 zone axis (inserted), in which B2 and DO_3 order phases are identified as super-lattice dots.

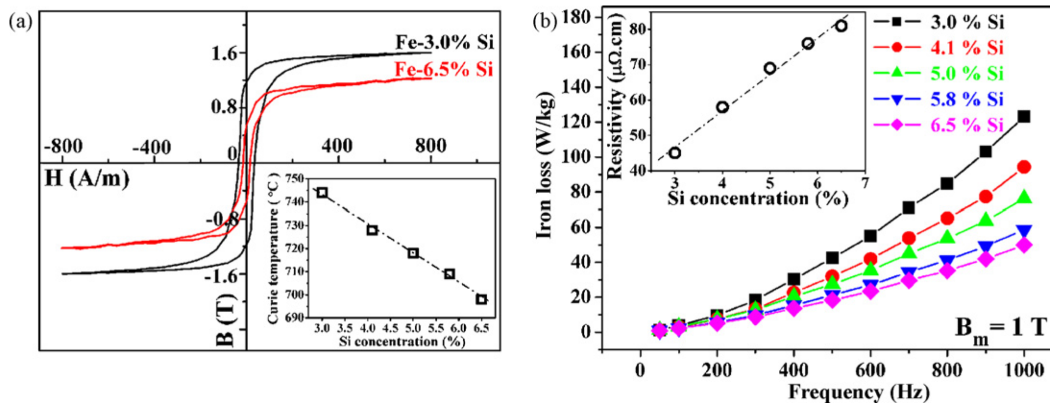

Fig. 6. Magnetic properties of the alloys (a) hysteresis loops of the Fe–3% Si and Fe–6.5% Si sheets fabricated in this work and inserted is Si content dependent Curie temperature and (b) Si dependent iron losses and electrical resistivity (inserted).

Table 2
Comparison of iron losses between the PVD-prepared Fe–6.5% Si alloys in this work and those by CVD method.

Sample	Thickness (mm)	Iron loss (W/kg)				
		$W_{10/50}$	$W_{10/400}$	$W_{5/1k}$	$W_{2/5k}$	$W_{1/10k}$
Fe–3% Si	0.35	1.09	21.6	21	57.1	42.5
Fe–6.5% Si (PVD)	0.35	0.69	13.7	12.9	29	25
Fe–6.5% Si (CVD)[a]	0.3	0.5	10.0	11.0	25.5	24.5

[a] Cited from Ref. [10].

is made between the present results and those fabricated from CVD method [5,10], as listed in Table 2. It should be mentioned that the CVD-fabricated sheet thickness is 0.30 mm, thinner than 0.35 mm (the thickness of the alloys in this work). As seen in Table 2, by taking into account the thickness effect on core losses [23,24], the Fe–6.5% Si prepared in this work demonstrates as low core losses as compared to the CVD-fabricated samples reported in the literature.

4. Conclusions

Fe–6.5% Si alloys with thickness of 0.35 mm have been fabricated by physical vapor deposition approach. FeSi layer was deposited on Fe–3% Si substrate to provide Si, which was penetrated into the substrate during subsequent annealing process. It is obtained that the Si penetration efficiency can be enhanced by reducing the FeSi layer thickness. Annealing time dependent cross-sectional Si distributions was simulated by DICTRA software, showing that Si content is distributed symmetrically along the cross-section and compositional gradient reaches zero with only 1 h annealing, which is in good agreement with experimental data. Microstructure observations reveal a dense and uniform microstructure for the prepared Fe–6.5% Si alloy, in which B2 and DO_3 order phases are observed. Iron losses of the PVD processed Fe–6.5% Si sheet are reduced by 40–50% as compared to the starting sheets and show as low values as those of the CVD-fabricated alloys.

References

[1] R.M. Bozorth, Ferromagnetism, Van Nostrand, New York, 1951, pp. 75–80.
[2] Y. Takada, M. Abe, S. Masuda, J. Inagaki, J. Appl. Phys. 64 (1988) 5367.
[3] T. Ros-Yáñez, D. Ruiz, J. Barros, Y. Houbaert, J. Alloy Compd. 369 (2004) 125.
[4] X.F. Bi, Y. Tanaka, K. Sato, K.I. Arai, K. Ishiyama, Y. Yamashiro, IEEE Trans. Magn. 32 (1996) 4818.
[5] H. Ninomiya, Y. Tanaka, A. Hiura, Y. Takada, J. Appl. Phys. 69 (1991) 5358.
[6] K. Arai, N. Tsuya, IEEE Trans. Magn. 16 (1980) 126.
[7] M. Enokizono, N. Teshima, K. Narita, IEEE Trans. Magn. 18 (1982) 1007.
[8] R.K. Roy, A.K. Panda, M. Ghosh, A. Mitra, R.N. Ghosh, J. Magn. Magn. Mater. 321 (2009) 2685.
[9] A.H. Kasama, C. Bolfarini, C.S. Kiminami, W.J. Botta Filho, Mater. Sci. Eng. A 449–451 (2007) 375.
[10] H. Haiji, K. Okada, T. Hiratani, M. Abe, M. Ninomiya, J. Magn. Magn. Mater. 160 (1996) 109.
[11] B. Navinšek, P. Panjan, I. Milošev, Surf. Coat. Technol. 116–119 (1999) 476.
[12] M. Hans, R. Büchel, M. Grischke, R. Hobi, M. Zäch, Surf. Coat. Technol. 123 (2000) 288.
[13] B. Schuhmacher, C. Schwerdt, U. Seyfert, O. Zimmer, Surf. Coat. Technol. 163–164 (2003) 703.
[14] M. Stueber, H. Holleck, H. Leiste, K. Seemann, S. Ulrich, C. Ziebert, J. Alloy Compd. 483 (2009) 321.
[15] J.M. Aldareguia, C.G. Rosales, J.G. Sevillano, Scripta Mater. 41 (1999) 729.
[16] C. Gelain, A. Cassuto, P. Le Goff, Oxid. Met. 3 (1971) 139.
[17] J.T. Law, J. Phys. Chem. 61 (1957) 1200.
[18] E. Rabkin, B. Straumal, V. Semenov, W. Gust, B. Predel, Acta Metall. Mater. 43 (1995) 3075.
[19] O. Kubachewski, Iron Binary Phase Diagrams, Springer-Velag, New York, 1982, pp. 136.
[20] J. Barros, J. Schneider, Y. Houbaert, J. Magn. Magn. Mater. 320 (2008) e389.
[21] J.H. Yu, J.S. Shin, J.S. Bae, et al., Mater. Sci. Eng. A307 (2001) 29.
[22] R.M. Bozorth, Ferromagnetism, Van Nostrand, New York, 1951, pp. 79.
[23] G. Bertotti, IEEE Trans. Magn. 24 (1988) 621.
[24] S.E. Zirka, Y.I. Moroz, P. Marketos, A.J. Moses, J. Magn. Magn. Mater. 320 (2008) 2504.